Diamond & Related Materials 104 (2020) 107744

Contents lists available at ScienceDirect

Diamond & Related Materials

journal homepage: www.elsevier.com/locate/diamond

Single crystal diamond gain mirrors for high performance vertical external cavity surface emitting lasers

Gergely Huszka[a], Nicolas Malpiece[b], Mehdi Naamoun[b], Alexandru Mereuta[b], Andreï Caliman[b], Grigore Suruceanu[b], Pascal Gallo[b], Niels Quack[a,*]

[a] École Polytechnique Fédérale de Lausanne, Switzerland
[b] LakeDiamond SA, Switzerland

ARTICLE INFO

Keywords:
Single crystal diamond
Reactive ion etching
High resolution electron microscopy
Optical properties characterization
Surface microscopy
Microstructure
Optical properties
Surface structure
Laser materials

ABSTRACT

We report on the design, fabrication and optical performance of gain mirrors in single crystal diamond substrates for vertical external cavity surface emitting lasers (VECSELs). VECSELs have gained attention recently due to their potential for high emission power in single mode with low beam divergence, yet their maximum output power remains typically limited due to thermal roll-over resulting from insufficient heat dissipation. In order to increase the heat transfer, we exploit the excellent thermal conductivity of single crystal diamond, which is assembled in direct contact with the active structure. The optical cavity is hereby defined by an output coupler and a high reflection grating structure etched into the diamond surface. We here present the design and microfabrication of a diffraction grating that was optimized to reflect light into the 0th order, therefore combining the role of a gain mirror and a heatsink at the same time. Our process involved metal mask deposition onto the diamond surface, e-beam lithography and reactive ion etching. Characterization showed reflection above 95% at a center wavelength of 1550 nm, potentially allowing the integration of the diamond mirror into a vertical external cavity surface emitting laser.

1. Introduction

Vertical external cavity surface emitting lasers (VECSELs) are semiconductor light sources that provide high optical output power simultaneously with excellent optical beam quality [1]. However, due to limited heat dissipation, VECSELs with emission wavelength above 1200 nm are typically limited in efficiency, with achievable output power typically limited to a few mW [2]. In order to improve their performance, several approaches have been demonstrated previously, including integration of heat spreaders to the gain mirrors [3], employing diamond [4] or silicon carbide [5], or decreasing the thermal resistance of the substrate and distributed Bragg reflector (DBR) by electroplated gold [6,7]. Despite these improvements emission power currently remains limited to 106 W at 1028 nm wavelength [8], 33 W at 1275 nm [9], and 1 W at 1560 nm [10].

We here pursue experimental investigations on the previously proposed double-diamond high-contrast-gratings VECSEL design [11], with the important modification, that the high contrast gratings (HCG) are etched directly into the diamond substrate instead of consisting of a deposited silicon layer, therefore enabling enhanced heat dissipation by the single crystal diamond. Our fabrication approach has been facilitated by the significant advances in fabrication technology of Chemical Vapor Deposition (CVD) single crystal diamond plates in recent years [12–15]. As a result, synthetically grown, high-quality single crystal diamond substrates are commercially available today from various suppliers (e.g. LakeDiamond, Element Six), typically processed by ultra-short pulse laser cutting and mechanical fine polishing [16,17]. Here, we demonstrate a microfabrication approach, based on metal mask deposition onto the diamond surface, e-beam lithography and reactive ion etching for pattern transfer.

In a typical VECSEL configuration, the active structure is attached to a distributed Bragg reflector (DBR) and the latter is in contact with a copper heatsink. Huang et al. presented a configuration in 2007, where the optical cavity was defined between 34 pairs of DBRs as bottom mirror and 4 pairs of DBR and an AlGaAs-based HCG as top mirror [18]. Compared to this design, in our configuration, all the DBRs of the bottom mirror were replaced by a HCG and an output coupler was employed as a top mirror. Furthermore, instead of applying a secondary layer as in [11], our proposed HCG is fabricated directly in the single crystal diamond, therefore integrating also the heatsink into the same

* Corresponding author.
E-mail address: niels.quack@epfl.ch (N. Quack).

https://doi.org/10.1016/j.diamond.2020.107744
Received 20 December 2019; Received in revised form 31 January 2020; Accepted 4 February 2020
Available online 04 February 2020

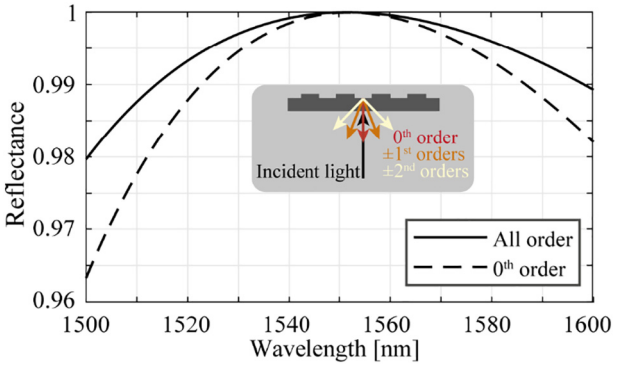

Fig. 1. Numerical simulation on the grating performance. RCWA-based reflection calculation for a diamond grating in air with dimensions bar width B = 592 nm, pitch P = 1455 nm and bar height H = 419 nm, when light approaches from the diamond substrate. The inset shows the schematic of the reflected orders.

component. While diffraction gratings in diamond have been demonstrated previously [19–21], we here specifically demonstrate a HCG design that was configured to achieve higher than 95% reflectance at operating wavelength of 1550 nm into the 0th order, which is an essential requirement for integration in VECSEL structures.

2. High contrast grating design

The initial parameters of the HCG were determined based on a previous study [11], and then were optimized by an iterative numerical simulation approach. The parameter search and optimization was performed based on the rigorous coupled wave analysis-based (RCWA) method [22] within a MatLab environment. The structure of the grating can be uniquely described by three variables, the width (B), the pitch (P) and the height of the bars (H). An algorithmic function was constructed that took into consideration the values of these three parameters and calculated the deviation of the 0th order reflection from one. By minimization of this function value, it was possible to find the combination of the parameters that resulted in the highest level of 0th order reflection, when the light approached the grating from the diamond substrate side (Fig. 1). This numerical analysis showed the set of B = 592 nm, P = 1455 nm and H = 419 nm to produce > 99.99% reflection. The result was confirmed by a finite element method (FEM) based simulation, validating the result with an independent numerical simulation method.

Furthermore, FEM based heat-transfer simulations were carried out in order to determine, how the physical dimensions of the diamond plates affect the performance of the VECSEL device. Based on the result of these studies, a 6 × 6 × 0.5 mm^3 diamond plate was identified to provide an optimal solution for both heat transfer and assembly.

3. Microfabrication and optical characterization methods

The single crystal diamond plates were obtained in two geometries, 3 × 3 × 0.25 mm (Element Six) and 6 × 6 × 0.5 mm (LakeDiamond). In both cases, the diamond plates were polished as described in our earlier work [23], cleaned with acetone and isopropanol before any further processing in a cleanroom. As a first step, the cleaned diamond surface was coated with a 150 nm thin layer of sputtered titanium (Fig. 2.A,F). This metal layer served a dual purpose as it acted as a conductive layer for e-beam lithography and as hard mask for diamond etching. The sputtering was followed by the pattern transfer, for which e-beam lithography was employed to reach a critical dimension of slightly below 600 nm with high fidelity. The diamond plates were spin-coated with hydrogen silsesquioxane (HSQ, Dow Corning XR-1541-006, at 2800 rpm) resulting in a 150 ± 10 nm thin layer. The design was

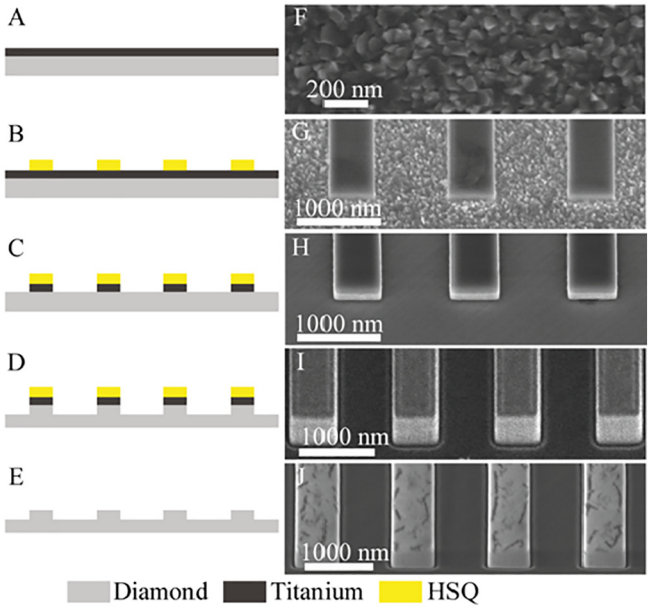

Fig. 2. Microfabrication process flow: A: Titanium deposition by sputtering on the diamond substrate. B: e-beam lithography to form HSQ mask on top of the titanium. C: Reactive Ion Etcher of the Titanium hard mask by chlorine chemistry. D: Reactive Ion Etching of Diamond by oxygen plasma. E: Hard mask removal, revealing the diamond grating. F–J: SEM images of the fabrication steps A–E, respectively.

then exposed with 3000 μC/cm^2 dose. For the development, the diamond plates were placed into 25% tetramethylammonium hydroxide (TMAH) aqueous solution for 4 min.

The quality of the e-beam lithography was investigated by optical microscope and by scanning electron microscope (SEM) qualitatively and by atomic force microscope (AFM) quantitatively (Fig. 2.B,G). Using the HSQ as mask, the titanium layer was then etched for 45 s in a STS Multiplex ICP reactive ion etcher using Cl_2/BCl_3 chemistry. During this process the coil power was set to 800 W, while the forward bias power was 150 W (Fig. 2.C,H). After opening the metal mask, the diamond could be etched directly, as we used the same tool for the latter etch, however, in our protocol, the diamond plates were removed from the etcher, washed in deionized water, inspected by SEM and then placed back into the same etcher. In order to etch the diamond, the configuration was changed to 400 W coil power, 200 W forward bias power and solely O_2 was employed for the plasma to generate the reactive ions. This setup allowed a diamond etch rate of 90–100 nm/min, depending on the feature dimensions, a phenomenon well documented in literature for dry etching processes as Aspect Ratio Dependent Etching (ARDE) [24,25] (Fig. 2.D,I).

The last step of the fabrication process consisted in the removal of the remaining mask materials from the surface by placing the diamond plates into 49% Hydrofluoric acid (HF) solution for 5 min. The fabricated gratings were subsequently measured by SEM and AFM to confirm the geometrical shapes and dimensions (Fig. 2.E,J).

Reflection measurements were conducted on an optical bench with the following setup (Fig. 3). A tunable laser (Agilent 8164A) was connected to a circulator (Thorlabs 6015-3-APC) that conducted the light to the sample through a gradient-index (GRIN) fiber collimator with anti-reflection coating (Thorlabs 50-1550A-APC). The sample was placed on a stage with two-axis tilt control and two-axis lateral translation control, while the working distance of the collimator was respected. The reflected light was collected by the fiber collimator and reached a power meter (HP 81531A) through the same circulator as detailed earlier. In order to calculate the power loss of our setup, a reference sample was always measured before the experiments. This

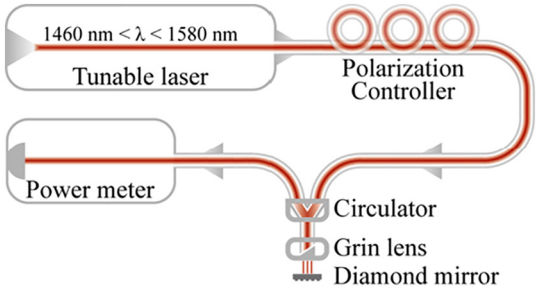

Fig. 3. Schematic of the reflection measurement setup. The tunable laser generates the wavelengths to be measured, which will reach the diamond mirror via a polarization controller, a circulator and a gradient-index (GRIN) lens. The reflected light is collected by the same GRIN lens and forwarded to the power meter via the circulator.

reference was a gold-coated (100 nm film) silicon wafer, for which an absolute reflectance of 98.66% at 1550 nm wavelength was assumed, based on literature data [26].

4. Results

The fabricated single crystal diamond HCGs were analyzed both qualitatively and quantitatively (Fig. 4.A). The SEM images showed well-defined structures of the extruded bars with smooth and near-vertical sidewalls.

In particular, as a result of the optimized etch process, we did not observe any micromasking in the trenches between the bars, which is a common challenge in nanostructuring of diamond [27](Fig. 4.B). In order to determine the exact dimensions of the three main design parameters, the HCG was measured quantitatively by AFM (Fig. 4.C). The target dimensions are reported with potential fabrication tolerances that would still allow the 0th order reflection to be higher than 99% and the measurement values are averages with their error bars as calculated standard deviation (for a sample number $n > 15$). Although the fabricated bar width turned out slightly smaller than the target, it remained within the tolerance region, while pitch and height deviated only a couple of nanometers from the target dimensions.

The SEM recordings reveal contrast differences on the top of the extruded bars (Fig. 4.B and Fig. 5.A). AFM measurements of the top of the bars, the trenches and the diamond surface outside the grating area are reported in Fig. 5.B as averages over $n = 15$ measurements with error bars as calculated standard deviation (n = 15). No significant difference between the three investigated areas was found. Furthermore, we could not observe any of the contrast difference-generated shapes on the AFM images; therefore, we concluded that the nature of the observed contrast variations are most likely caused by a surface modification rather than residues e.g. from the masking material.

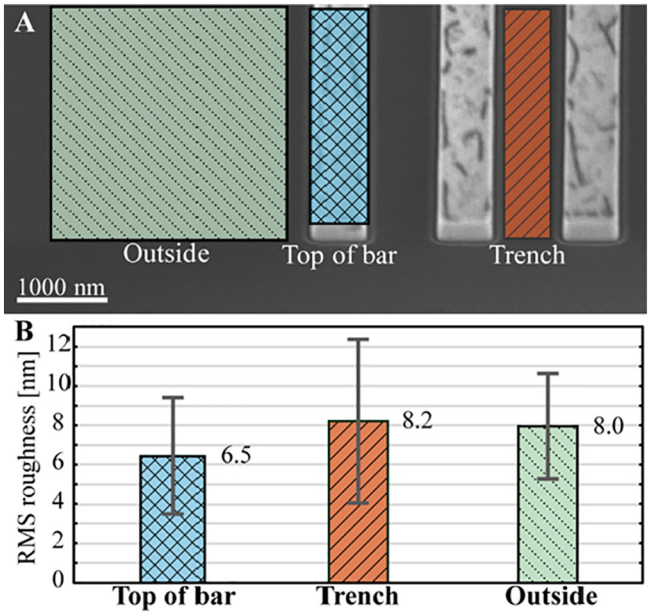

Fig. 5. Surface roughness measurements on the HCG. A: SEM recording with indication of the measurement areas. B: AFM measurement of the surface roughness with averages and error bars as standard deviation over n = 15 measurements.

Optical performance was experimentally assessed employing the characterization setup described in the methods section. The spectral response for the wavelength range 1550 ± 3 nm was recorded with 0.02 nm increment both for the gold reference and for the HCG. As the grating was designed to work with TE polarized light, the polarization controller was set accordingly to maximize the optical response, as well as the tilted stage that was adjusted to provide perpendicular surface relative to the GRIN fiber collimator. Since the reflection of the gold surface is independent from the polarization, these adjustments did not influence the reference reflectivity. The results are summarized in Fig. 6. Our gold reference provided 98.66% reflection, while the fabricated HCG reached 95.85% at 1550 nm wavelength. The periodic variation in recorded intensity, is resulting from the Fabry–Pérot cavity between the diamond plate top and bottom surfaces (see Appendix A).

5. Discussion and conclusion

The reflectivity of the single crystal high contrast grating was experimentally determined to be 95.85% at 1550 nm, which is ~3%

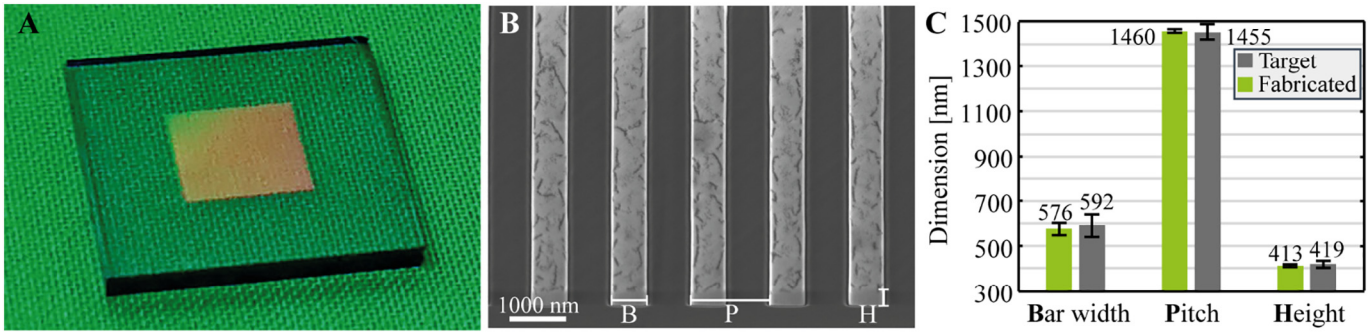

Fig. 4. The fabricated single crystal diamond high contrast grating (HCG). A: Photograph of the HCG on a 6 × 6 × 0.5 mm^3 diamond plate. B: SEM images of the HCG, indicating the three main design parameters (Bar width, Pitch, Height). C: Results of AFM measurements on the fabricated HCG. The grey bars represent the target dimensions, while the green bars reflect the measured dimensions. Error bars mark the tolerance for > 99% reflection in the case of the target values, while they mark standard deviation ($n > 15$) for the measured values. (For interpretation of the references to colour in this figure legend, the reader is referred to the web version of this article.)

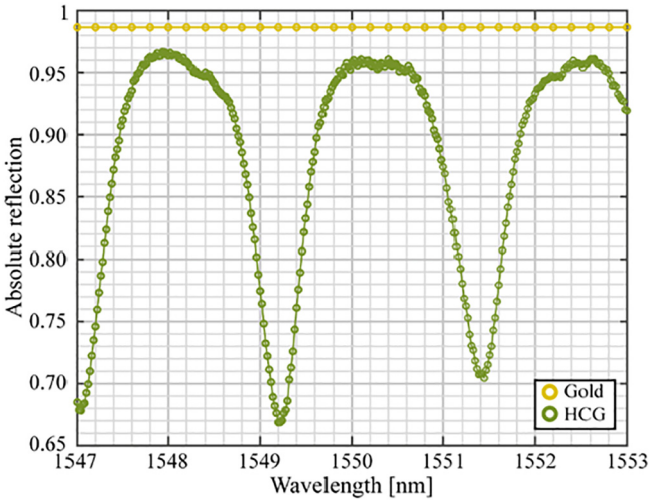

Fig. 6. Results of the reflection measurements. Data points were measured between 1547 and 1553 nm with 0.02 nm increment. The gold reference (gold marks) was a 100 nm thin film deposited on a silicon wafer, while the HCG (green marks) was the fabricated single crystal diamond grating. (For interpretation of the references to colour in this figure legend, the reader is referred to the web version of this article.)

lower than designed. This discrepancy can be attributed to a combination of imperfections resulting from the fabrication process, such as surface roughness leading to scattering losses, non-verticality of the grating bars or the residual trenches observed at the bottom edges of the grating bars, and tolerances resulting from the measurement method, such as imperfect alignment of the grating with respect of the collimating lens.

In summary, we have presented an advanced diamond microfabrication process enabling structuring of single crystal diamond surfaces with pattern dimensions of 100 nm–1500 nm, with precision of ~10 nm. Based on this process, we have experimentally demonstrated a high contrast grating etched into a single crystal diamond yielding reflectivity exceeding 95% at a wavelength of 1550 nm. Such high contrast gratings in diamond are potentially excellent candidates for integration in VECSEL structures to enable high power lasing structures by exploiting the high thermal conductivity of single crystal diamond. This technique can further be extended to create various mechanical and optical components, such as lenses, gratings, or diffractive optical elements.

Declaration of competing interest

LakeDiamond SA is interested in the commercial exploitation of the device described in the manuscript.

All other authors declare that they have no known competing financial interests or personal relationships that could have appeared to influence the work reported in this paper.

Acknowledgements

The project is supported by the Swiss Space Center, and by LakeDiamond SA, a commercial supplier of cut and polished high-purity single crystal diamond substrates. All microfabrication steps were performed at the Center for Micro- and Nanofabrication (CMi) at EPFL. The authors gratefully acknowledge the technical support of the CMi management and staff.

Funding

The authors acknowledge funding by the Swiss State Secretariat for Education, Research and Innovation and by the Swiss National Science Foundation under grant no. 157566 and 183717.

Appendix A

The free spectral range calculation for the Fabry-Pérot cavity was started from the equation $\Delta\nu \approx \frac{c}{n(\lambda)L}$ when the dispersion is negligible, i.e. $\frac{\partial n}{\partial \lambda} = 0$, which was found in this case as $\approx -0.00879\,\frac{1}{\mu m}$. Rearranging the equation yields:

$$L = \frac{c}{n(\lambda)\Delta\nu} = \frac{c}{n(\lambda)\left|\frac{c}{\lambda_1} - \frac{c}{\lambda_2}\right|} = 456.223\ \mu\text{m}$$

when $|\lambda_1 - \lambda_2| \approx 2.2\,nm$, which was found for several measurements. For a standing wave cavity, the physical length is half of L, which translates to 228.112 μm. This was in good correspondence with the datasheet of the diamond plate, which stated that the plate thickness is 250 ± 50 μm.

References

[1] Y. Suematsu, K. Iga, Semiconductor lasers in photonics, J. Light. Technol. 26 (2008) 1132–1144, https://doi.org/10.1109/JLT.2008.923615.
[2] A. Caliman, A. Mereuta, G. Suruceanu, V. Iakovlev, A. Sirbu, E. Kapon, 8 mW fundamental mode output of wafer-fused VCSELs emitting in the 1550-nm band, Opt. Express 19 (2011) 16996–17001, https://doi.org/10.1364/OE.19.016996.
[3] W.J. Alford, T.D. Raymond, A.A. Allerman, High power and good beam quality at 980 nm from a vertical external-cavity surface-emitting laser, JOSA B 19 (2002) 663–666, https://doi.org/10.1364/JOSAB.19.000663.
[4] J.-M. Hopkins, S.A. Smith, C.W. Jeon, H.D. Sun, D. Burns, S. Calvez, M.D. Dawson, T. Jouhti, M. Pessa, 0.6 W CW GaInNAs vertical external-cavity surface emitting laser operating at 1.32 μm, Electron. Lett. 40 (2004) 30–31, https://doi.org/10.1049/el:20040049.
[5] J.E. Hastie, J.-M. Hopkins, S. Calvez, C.W. Jeon, D. Burns, R. Abram, E. Riis, A.I. Ferguson, M.D. Dawson, 0.5-W single transverse-mode operation of an 850-nm diode-pumped surface-emitting semiconductor laser, IEEE Photon. Technol. Lett. 15 (2003) 894–896, https://doi.org/10.1109/LPT.2003.813446.
[6] A.R. Zakharian, J. Hader, J.V. Moloney, S.W. Koch, P. Brick, S. Lutgen, Experimental and theoretical analysis of optically pumped semiconductor disk lasers, Appl. Phys. Lett. 83 (2003) 1313–1315, https://doi.org/10.1063/1.1601672.
[7] M. Devautour, A. Michon, G. Beaudoin, I. Sagnes, L. Cerutti, A. Garnache, Thermal management for high-power single-frequency tunable diode-pumped VECSEL emitting in the near- and mid-IR, IEEE J. Sel. Top. Quantum Electron. 19 (2013), https://doi.org/10.1109/JSTQE.2013.2245104 (1701108–1701108).
[8] B. Heinen, T.-L. Wang, M. Sparenberg, A. Weber, B. Kunert, J. Hader, S.W. Koch, J.V. Moloney, M. Koch, W. Stolz, 106 W continuous-wave output power from vertical-external-cavity surface-emitting laser, Electron. Lett. 48 (2012) 516–517, https://doi.org/10.1049/el.2012.0531.
[9] T. Leinonen, V. Iakovlev, A. Sirbu, E. Kapon, M. Guina, 33 W continuous output power semiconductor disk laser emitting at 1275 nm, Opt. Express 25 (2017) 7008, https://doi.org/10.1364/OE.25.007008.
[10] A. Rantamäki, J. Rautiainen, A. Sirbu, A. Mereuta, E. Kapon, O.G. Okhotnikov, 156 μm 1 watt single frequency semiconductor disk laser, Opt. Express 21 (2013) 2355, https://doi.org/10.1364/OE.21.002355.
[11] V. Iakovlev, J. Walczak, M. Gębski, A.K. Sokół, M. Wasiak, P. Gallo, A. Sirbu, R.P. Sarzala, M. Dems, T. Czyszanowski, E. Kapon, Double-diamond high-contrast-gratings vertical external cavity surface emitting laser, J. Phys. Appl. Phys. 47 (2014) 065104, , https://doi.org/10.1088/0022-3727/47/6/065104.
[12] A. Toros, M. Kiss, T. Graziosi, H. Sattari, P. Gallo, N. Quack, Precision micro-mechanical components in single crystal diamond by deep reactive ion etching, Microsyst. Nanoeng. 4 (2018), https://doi.org/10.1038/s41378-018-0014-5.
[13] M. Kiss, T. Graziosi, N. Quack, Trapezoidal diffraction grating beam splitters in single crystal diamond, in: A.L. Glebov, P.O. Leisher (Eds.), Compon. Packag. Laser Syst. IV, SPIE, San Francisco, United States, 2018, p. 55, , https://doi.org/10.1117/12.2290557.
[14] M. Kiss, T. Graziosi, A. Toros, T. Scharf, C. Santschi, O.J.F. Martin, N. Quack, High-

quality single crystal diamond diffraction gratings fabricated by crystallographic etching, Opt. Express 27 (2019) 30371–30379, https://doi.org/10.1364/OE.27.030371.
[15] M. Schwander, K. Partes, A review of diamond synthesis by CVD processes, Diam. Relat. Mater. 20 (2011) 1287–1301, https://doi.org/10.1016/j.diamond.2011.08.005.
[16] M. Polikarpov, V. Polikarpov, I. Snigireva, A. Snigirev, Diamond X-ray refractive lenses with high acceptance, Phys. Procedia 84 (2016) 213–220, https://doi.org/10.1016/j.phpro.2016.11.037.
[17] R. Mildren, J. Rabeau, Optical Engineering of Diamond, John Wiley & Sons, 2013.
[18] M.C.Y. Huang, Y. Zhou, C.J. Chang-Hasnain, A surface-emitting laser incorporating a high-index-contrast subwavelength grating, Nat. Photonics 1 (2007) 119–122, https://doi.org/10.1038/nphoton.2006.80.
[19] T.V. Kononenko, D.N. Sovyk, P.A. Pivovarov, V.S. Pavelyev, A.V. Mezhenin, K.V. Cherepanov, M.S. Komlenok, V.R. Sorochenko, A.A. Khomich, V.P. Pashinin, E.E. Ashkinazi, V.G. Ralchenko, V.I. Konov, Fabrication of diamond diffractive optics for powerful CO2 lasers via replication of laser microstructures on silicon template, Diam. Relat. Mater. (2019) 107656, , https://doi.org/10.1016/j.diamond.2019.107656.
[20] E. Vargas Catalan, P. Forsberg, O. Absil, M. Karlsson, Controlling the profile of high aspect ratio gratings in diamond, Diam. Relat. Mater. 63 (2016) 60–68, https://doi.org/10.1016/j.diamond.2015.08.007.
[21] J. Schmitt, W. Nelissen, U. Wallrabe, F. Völklein, Implementation of smooth nanocrystalline diamond microstructures by combining reactive ion etching and ion beam etching, Diam. Relat. Mater. 79 (2017) 164–172, https://doi.org/10.1016/j.diamond.2017.09.014.
[22] J.P. Hugonin, P. Lalanne, Reticolo Software for Grating Analysis, Institut d'Optique, Orsay, France, 2005.
[23] S. Mi, A. Toros, T. Graziosi, N. Quack, Non-contact polishing of single crystal diamond by ion beam etching, Diam. Relat. Mater. 92 (2019) 248–252, https://doi.org/10.1016/j.diamond.2019.01.007.
[24] O. Antonin, R. Schoeppner, M. Gabureac, L. Pethö, J. Michler, P. Raynaud, T. Nelis, Nano crystalline diamond MicroWave Chemical Vapor Deposition growth on three dimension structured silicon substrates at low temperature, Diam. Relat. Mater. 83 (2018) 67–74, https://doi.org/10.1016/j.diamond.2018.01.007.
[25] P. Forsberg, M. Karlsson, High aspect ratio optical gratings in diamond, Diam. Relat. Mater. 34 (2013) 19–24, https://doi.org/10.1016/j.diamond.2013.01.009.
[26] D.I. Yakubovsky, A.V. Arsenin, Y.V. Stebunov, D.Y. Fedyanin, V.S. Volkov, Optical constants and structural properties of thin gold films, Opt. Express 25 (2017) 25574–25587, https://doi.org/10.1364/OE.25.025574.
[27] M.-L. Hicks, A.C. Pakpour-Tabrizi, R.B. Jackman, Diamond etching beyond 10 μm with near-zero micromasking, Sci. Rep. 9 (2019) 15619, , https://doi.org/10.1038/s41598-019-51970-8.